

Effects of Chemical Kinetic Mechanism on Pollutant NO Prediction of Turbulent Diffusion Flame using Large Eddy Simulation

Rahmat Waluyo^a, Kazuma Kunihara^a, Muhammad Aziz^{b,*}

^aDepartment of Mechanical Engineering, The University of Tokyo, 1-1-1 Yayoi, Bunkyo-ku, Tokyo, 113-0032, Japan

^bInstitute of Industrial Science, 4-6-1 Komaba, Meguro-ku, Tokyo, 153-8505, Japan

maziz@iis.u-tokyo.ac.jp

Large eddy simulation (LES) and detailed chemical kinetic mechanisms are employed to obtain a high-resolution and accurate prediction of temperature and chemical species mass fraction inside the turbulent diffusion flame of a model burner. Open-source software OpenFOAM[®] with embedded solver reactingFoam is used to discretize and solve Favre-filtered governing equations consisting of mass, momentum, species, and energy transport equations. Partially-stirred reactor (PaSR) model is used to provide subgrid scale (SGS) closure of turbulence-chemistry interaction (TCI) on mass and energy transport equations. Temperature and species measurement data of combustion case H3 taken from a model burner developed by the German Aerospace Center (DLR) and TU Darmstadt are used to validate simulation results. LES turbulence submodel of dynamic *k*-equation is employed to provide SGS closure for unresolved eddies through the eddy viscosity model. Detailed chemical kinetic mechanisms used include GRI-Mech 3.0 and Mevel mechanisms. A dynamic load balancing (DLB) technique is implemented to accelerate the parallel calculation of chemical source terms. The prediction accuracy of minor species, including radical OH and pollutant NO, depends on the chemical kinetic mechanism. More elaborated nitrogen reactions in GRI-Mech 3.0 result in better NO prediction than Mevel mechanism. Finally, the potential of applying an optimized numerical setup with the least deviation from experimental measurement is highlighted.

1. Introduction

An international agreement to limit global temperature increase has prompted countries to reduce carbon emissions in the energy sector. One strategy to facilitate this energy transition involves fuel substitution on the established mode of energy utilization, such as combustion. Among proposed fuel alternatives, hydrogen appears promising due to the possibility of attaining zero carbon emission throughout the hydrogen life cycle. Consequently, a significant increase in hydrogen-based energy demand is attributed to energy transformation, which includes a gradual process of fuel substitution on existing power generation infrastructure, such as hydrogen cofiring with hydrocarbon fuel or the development of combustion devices dedicated to pure hydrogen fuel (Funke et al., 2019).

However, incompatibilities between hydrogen and existing hydrocarbon engines might result in emission and safety concerns. In the absence of carbon, the main pollutant of hydrogen-based renewable fuels is the generated NO which originates from nitrogen air or fuel. Experimental characterization of NO_x emission was attempted with observed low NO emission at a slightly rich equivalence ratio (Mashruk et al., 2021). The issue of NO emission has become important since NO is a key precursor of N₂O, a greenhouse gas with a global warming potential 273 times the CO₂. Consequently, the design and optimization of combustion devices to reduce dangerous emissions are necessary to facilitate hydrogen adoption as a key strategy in larger energy transition schemes. Optimization of combustion devices requires an accurate description of flame during combustion. However, a complex interaction between turbulence and chemical reactions inside the combustion chamber makes a straightforward analytical solution of governing equations unlikely to be achieved. To overcome this problem, researchers employ a numerical approach to approximate combustion phenomena.

However, the wide range of time and length scales related to turbulent eddies make the computational cost of direct numerical simulation (DNS) prohibitively expensive. Attempts to reduce computational cost have been made by solving filtered or averaged governing equations that correspond to large eddy simulation (LES) and Reynolds-averaged Navier-Stokes (RANS) simulation. These approaches lead to the evaluation of subgrid-scale or fluctuating quantities in terms of filtered or mean value, which is the essence of the turbulence model. Comparison between LES and RANS in combustion modeling shows the advantages of LES to resolving instantaneous behavior on flame stabilization.

Similarly, the interaction between turbulence and chemical reactions must also be modeled as a function of filtered/averaged quantities to achieve affordable flame simulation. Several approaches have been attempted to model turbulence-chemistry interaction. The flamelet model approximates flame as a thin geometric surface whose area is proportional to the reaction rate. The validity of this model is traditionally attributed to flames with low turbulence intensity, where turbulent eddies wrinkle flame below their stretching limit (Borghi, 1985). On the other hand, the turbulent mixing model accommodates higher turbulence intensity by taking into account the mixing due to turbulent eddies passing through the flame front. Several flame models from this category include the popular eddy-break-up model (Spalding, 1977) and the partially-stirred reactor model (Li et al., 2018).

Along with DNS data for verification, experimental data is also needed to validate the numerical model employed in the flame simulation. The International Workshop on Measurement and Computation of Turbulent Flames is a global cooperation framework providing experimental data for several model burners. Among these, the model burner developed by German Aerospace Center (DLR) Stuttgart exhibits strong turbulence-chemistry interaction with a relatively simple configuration. The experimental measurement of this burner has been frequently used as a validation dataset for hydrogen diffusion flame simulation by the previous authors (Zhou et al., 2016).

Apart from the accuracy aspect, the computational cost of performing a numerical simulation of combustion also needs to be considered. The current method for solving discretized governing equations of reacting flows involves splitting between chemistry and transport calculation, enabling each calculation to be performed in parallel. Recent improvement in parallel computing introduces dynamic load balancing (DLB) (Tekgöl et al., 2021) to improve the parallelization performance of reacting flow simulation. This development offers significant computational cost reduction and opens the possibility of more demanding turbulent flame simulation.

Considering the absence of carbon in hydrogen fuel, the control and reduction of NO emissions as the main pollutant of hydrogen combustion need to be achieved through the optimized design of the combustion chamber. Accurate prediction of NO through LES of hydrogen/air model burner is required to gain an understanding of the parameter that influences NO prediction. To the best of the authors' knowledge, an accurate simulation of NO emission has not been achieved for the case of hydrogen/air turbulent diffusion/non-premixed flame (TNF). This research aims to accurately predict NO emission and elaborate the effects of chemical kinetics mechanism on NO prediction of hydrogen/air TNF LES enhanced with parallel computing.

2. Methods

2.1 Governing equations, and simulation model

Reacting gas flow is governed by compressible Navier-Stokes equations, which consist of continuity, momentum, species, and energy transport equations. Favre-filtered LES formulations of these equations for N chemical species are given as:

$$\frac{\partial \bar{\rho}}{\partial t} + \frac{\partial (\bar{\rho} \tilde{u}_j)}{\partial x_j} = 0 \quad (1)$$

$$\frac{\partial (\bar{\rho} \tilde{u}_i)}{\partial t} + \frac{\partial (\bar{\rho} \tilde{u}_i \tilde{u}_j)}{\partial x_j} = \frac{\partial}{\partial x_j} [-\bar{p} \delta_{ij} + \bar{\rho} \tilde{u}_i \tilde{u}_j - \bar{\rho} \tilde{u}_i \tilde{u}_j + \bar{\rho} \tilde{S}_{ij}] \quad (2)$$

$$\frac{\partial (\bar{\rho} \tilde{Y}_k)}{\partial t} + \frac{\partial (\bar{\rho} \tilde{u}_i \tilde{Y}_k)}{\partial x_j} = \frac{\partial}{\partial x_j} [\bar{\rho} \tilde{u}_j \tilde{Y}_k - \bar{\rho} \tilde{u}_j \tilde{Y}_k + \bar{\rho} D_k \frac{\partial \tilde{Y}_k}{\partial x_j}] + \bar{\omega}_k, \quad k = 1, \dots, N \quad (3)$$

$$\frac{\partial (\bar{\rho} \tilde{h})}{\partial t} + \frac{\partial (\bar{\rho} \tilde{u}_j \tilde{h})}{\partial x_j} = \frac{D\bar{p}}{Dt} + \frac{\partial}{\partial x_j} [\bar{\rho} \tilde{u}_j \tilde{h} - \bar{\rho} \tilde{u}_j \tilde{h} + \bar{\rho} \alpha \frac{\partial \tilde{h}}{\partial x_j}] + \bar{\omega}_h \quad (4)$$

where $\bar{\rho}$ [$kg \cdot m^{-3}$], \tilde{u}_i [$m \cdot s^{-1}$], \bar{p} [$kg \cdot m^{-1} s^{-2}$], \tilde{S}_{ij} [s^{-1}], \tilde{Y}_k [-], and \tilde{h} [$m^2 \cdot s^{-2}$] represents density, velocity, pressure, strain rate, mass fraction of species k , and specific enthalpy of the mixture. The overbar ($\bar{\quad}$) indicates unweighted filtered quantities, while the tilde ($\tilde{\quad}$) denotes density-weighted filtered quantities. Mixture-averaged

values of kinematic viscosity and thermal diffusivity are denoted by $\nu[m^2.s^{-1}]$ and $\alpha[m^2.s^{-1}]$. The production rate of species k due to chemical reactions is represented by the source term $\bar{\omega}_k[s^{-1}]$, while heat release rate (HRR) in Eq(4) is related to chemical source term by $\bar{\omega}_h = \sum_k^N \Delta h_{f,k}^0 \bar{\omega}_k$, where $\Delta h_{f,k}^0[m^2.s^{-2}]$ indicate species standard enthalpy of formation. The mixture's sensible enthalpy (h) is given by the following expression.

$$h_k = \int_{T_{ref}}^T c_p dT \quad (5)$$

where $c_p[m^2.s^{-2}.K^{-1}]$ represents mixture-averaged constant-pressure specific heat. Assumption of unity Lewis number is taken for all species implying $D = \alpha$. The set of governing equations is complemented by the ideal gas law.

The finite volume method (FVM) embedded in open-source software OpenFOAM-8[®] with solver reactingFoam is utilized to solve Eqs(1)–(4) with 2nd order implicit time discretization scheme. Combinations of pressure implicit with the splitting of operators (PISO) and the semi-implicit method for pressure-linked equations (SIMPLE) form the PIMPLE algorithm that is used to achieve pressure-velocity coupling. Central differencing schemes are used to discretize the diffusion terms, while the non-linear dissipative Gamma scheme is utilized to discretize the convective terms.

The effects of sub-grid scale (SGS) eddies are approximated by an eddy viscosity model whose turbulent viscosity is modeled further by a dynamic k -equation submodel (Kim and Menon, 1995). In dynamic k -equation, turbulent viscosity is calculated from algebraic expression $\nu_T = C_k \Delta \sqrt{k}$ where $\Delta[m]$ and $k[m^2.s^{-2}]$ are LES grid length and SGS kinetic energy. Simulation parameter C_k is calculated and determined dynamically through filtering operation. Large timescale differences between flow and chemistry lead to the use of a partially stirred reactors (PaSR) combustion model, which employs an operator-splitting technique to divide the calculation of species mixing and chemical reaction inside each computational cell. The assumption in this model is manifested in an approximation of filtered chemical source term $\bar{\omega}_k$.

2.2 Studied burner and simulation setup

The flame considered in the current research is based on a TNF burner developed by DLR, having a jet nozzle diameter (D) of 8 mm. Combustion case H3 which uses nitrogen-diluted hydrogen fuel with a volume fraction of 50 % H_2 and 50 % N_2 and has jet exit velocity (u_{jet}) of 34.8 m/s corresponding to Reynolds number (Re) of 10,000, is adopted as the base case in this study. The flame is supplied with co-flow air through a 140 mm outer cylinder at a velocity of 0.3 m/s, which acts as an oxidiser.

The computational domain consists of a three-dimensional cylinder along interval $(0, 50D)$ in the axial (x) direction and $(0, 8.75D)$ in the radial direction (r), as shown in Figure 1a. The domain is discretized into hexahedral mesh elements with a detailed view shown in Figure 1b. The area near the axis has a square shape with a slightly curved side.

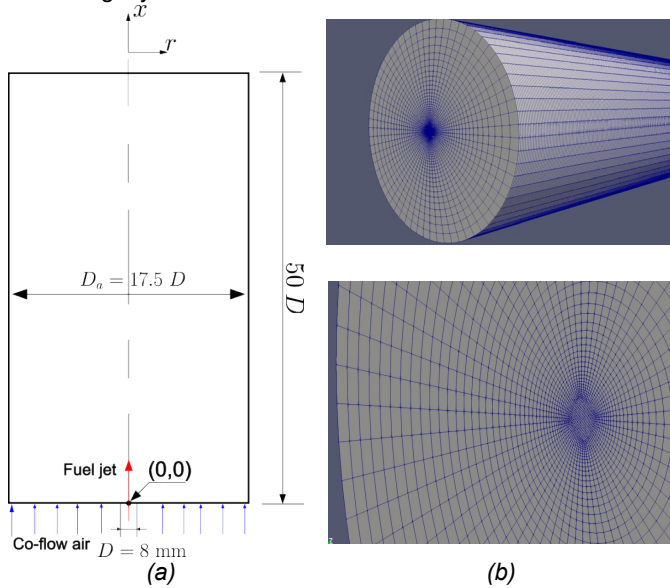


Figure 1: (a) Schematic of the burner and (b) details of the computational domain.

Combustion is initiated by setting a high temperature (2,200 K) in a small region near the fuel inlet. In this simulation, the velocity profile of fuel flow is defined by fully developed pipe flow where the bulk velocity equals u_{jet} . Dirichlet-type boundary conditions with fixed values are imposed on the velocity and temperature of an air inlet. Both fuel and air temperature at the inlet are set at 292 K. Neumann-type boundary condition with zero gradients for species, and temperature is used at the azimuthal boundary plane. The wave-transmissive boundary condition is used on pressure at the outlet and azimuthal plane to prevent pressure wave reflection back to the computational domain. Similarly, the mixed boundary condition of gradient and fixed value is imposed on the velocity at the outlet and azimuthal plane to prevent backflow. Figure 2 illustrates the location of boundary conditions discussed in previous passage.

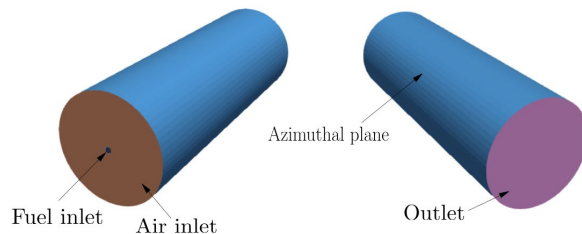


Figure 2: Boundary conditions of computational domain.

2.3 Chemical mechanism and computational load balancing

The widely known mechanism developed by Gas Research Institute (GRI), GRI-Mech, has been designed to model chemistry source terms of hydrocarbon combustion. In this work, the current version of the GRI-Mech 3.0 mechanism (referred to as GRI-3) is adopted, which consists of 53 species and 325 reactions, including 28 reversible reactions for the H_2/O_2 kinetic subset. In addition, the chemical mechanism developed by Mevel et al. (2009) (hereafter referred to as the Mevel mechanism) was designed to model the chemical reactions of a hydrogen-nitrous oxide mixture. Part of Mevel mechanism which consists of 14 species and 42 reactions, including NO formation, was extracted from the detailed Mevel mechanism to model hydrogen-air LES TNF in the current work. A partial mechanism is available online and can be loaded using Cantera.

Highly non-linear characteristics of chemical kinetic often lead to a large variation of convergence rates of ODE solver, causing high load imbalance across multiprocessor systems. This issue was addressed by implementing DLBFoam (Tekgöl et al., 2021), a DLB library for OpenFOAM that facilitates chemistry load balancing between processors that can effectively reduce the processor waiting time. Table 1 summarizes the numerical setups used in each simulation case.

Table 1: Summary of numerical setups used in each simulation case

Case	DLB	Chemical mechanism	Mesh size
A	ON	Mevel	601,600
B	ON	Mevel	1,203,200
C	ON	Mevel	2,406,400
D	ON	GRI-3	1,203,200

3. Results and discussion

3.1 Verification and validation

Verification of combustion simulation is carried out by grid independence test, which compares the simulated temperature and species mass fraction between the coarse and refined mesh. In addition, a comparison between quantities measured by the experiment and simulated quantities is needed to validate the combustion simulation. Figure 3 shows a comparison between simulation results and experimental measurement using Raman spectroscopy by DLR (Cheng et al., 1995) and combined Raman-laser induced fluorescence (LIF) method conducted in TU Darmstadt (Tacke et al., 1998).

Prediction of temperature and major species mass fractions (H_2 , O_2 , and H_2O) shows satisfactory convergent trend to experimental measurement. However, simulated NO fails to approximate measured values albeit the increase of number of cells mesh. This observation is due to lack of nitrogen chemistry in the employed partial Mevel mechanism which motivates adoption of detailed GRI-3 mechanism in the next section.

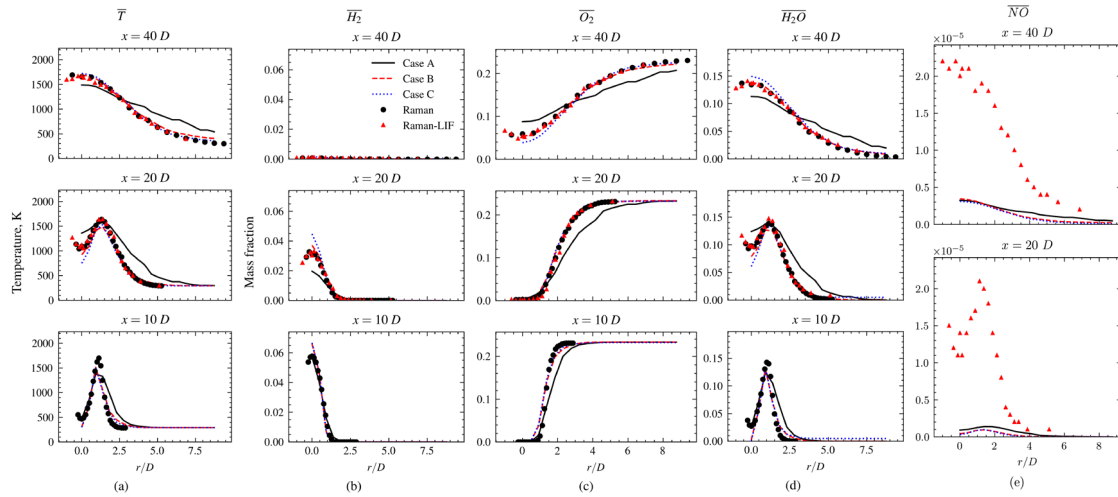


Figure 3: Radial plot of mean simulated (lines) and measured (scatter) thermochemical scalar for combustion case H3. Coarse (case A), intermediate (case B) refined (case C) mesh is used to predict (a) temperature, (b)-(d) major species (H_2 , O_2 , and H_2O), and (e) minor species (NO) at different stream-wise positions.

Most simulated quantities obtained using finer mesh (~ 2.4 million cells) coincide with experimental data more than the coarse mesh (~ 0.6 million cells) since the increase in spatial resolution leads to more resolved eddies. The use of intermediate mesh exhibits a grid independence point where additional mesh refinement would not lead to a significant increase in simulation result convergence to experimental data. Further simulation to address the low accuracy of NO prediction will be conducted with different chemical mechanisms on the intermediate mesh.

3.2 Chemical mechanism comparison

Figure 4 shows the simulated temperature and species mass fraction distribution using Mevel and GRI-3 mechanisms. Both mechanisms give a similar prediction of temperature and major species mass fractions. However, the profile of simulated minor species depends on the employed mechanism. The GRI-3 mechanism predicts pollutant NO better than the Mevel mechanism, which underpredicts NO measurement. This fact can be attributed to more elaborate nitrogen reactions included in the GRI-3 mechanism.

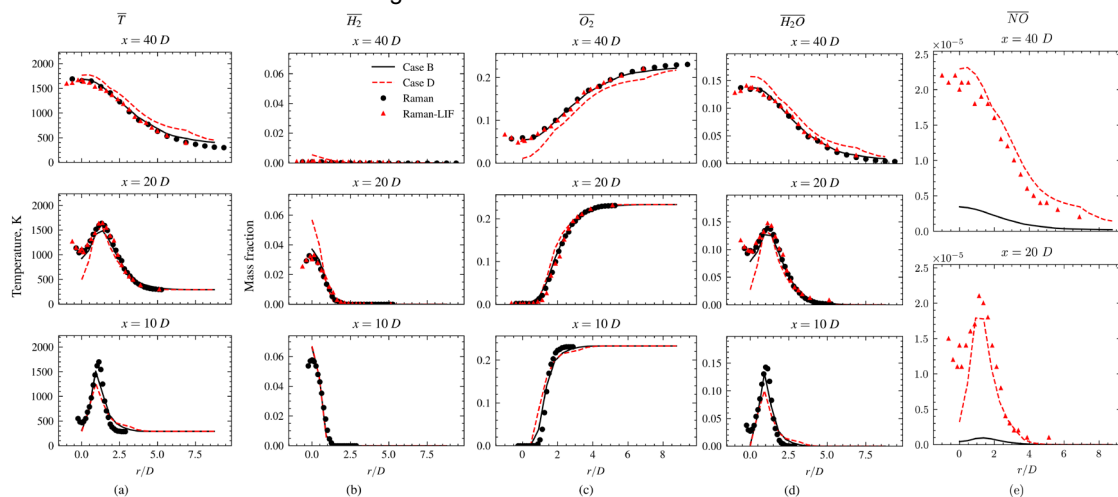


Figure 4: Radial plot of mean simulated (lines) and measured (scatter) thermochemical scalar for combustion case H3. Mevel (case B) and GRI-3 (case D) mechanism is used to predict (a) temperature, (b)-(d) major species (H_2 , O_2 , and H_2O), and (e) minor species (NO) at different stream-wise positions.

It is noted that the detailed mechanism GRI-3 deviates from both experimental measurements of temperature and major species near the burner axis. This observation becomes more apparent at a downstream location

where the Mevel mechanism agrees to experiment values better than GRI-3. Another interesting point is the significant increase in prediction accuracy of pollutant NO by employing detailed mechanisms. More elaborate nitrogen chemistry embedded in the GRI-3 mechanism evidently leads to better agreement with measured NO mass fraction. A previous attempt to achieve an accurate simulation of NO emission was made on a partially premixed H₂/air diffusion flame (Capurso et al., 2023). To the best of the author's knowledge, recent results show the first accurate NO prediction with significant accuracy for the case of H₂/air turbulent non-premixed flame LES.

4. Conclusions

LES of hydrogen/air TNF from DLR case H3 has been conducted in this research. Obtained scalar field from simulation with grid-independent simulation setup converges with experimental measurement, which indicates simulation has been verified and validated. A comparison of simulated NO emission between LES with different chemical mechanisms was made. Important points from this research are summarized by the following points:

1. The proposed simulation setup using an intermediate mesh with 1,203,200 cells exhibits grid-independent results, which adequately converge to the experimental measurement of temperature and mass fraction.
2. The more elaborate nitrogen chemistry in the detailed mechanism GRI-3 mechanism yields a more accurate prediction of pollutant NO in LES relative to the partial Mevel mechanism.

Acknowledgments

This research is supported by the JST/JICA SATREPS program, grant ID JPMJSA2204 and Public-Private Support Program for Discovery of Young Researchers NEDO grant ID 22688970. The computational resource is provided by the Initiative on Recommendation Program for Young Researchers and Woman Researchers, Information Technology Center, The University of Tokyo.

References

- Borghesi R., 1985, On the Structure and Morphology of Turbulent Premixed Flames, *Recent Advances in Aerospace Sciences*, 117–138.
- Capurso T., Laera D., Riber E., Cuenot B., 2023, NO_x pathways in lean partially premixed swirling H₂-air turbulent flame, *Combustion and Flame*, 248.
- Cheng T.-C., Fruechtinger G., Neuber A., Lipp F., Hassel E. P., Janicka J., 1995, Experimental data base for numerical simulations of turbulent diffusion flames, *Engineering Research*, 6, 165–171.
- Funke H.H.-W., Beckmann N., Abanteriba S., 2019, An overview on dry low NO_x micromix combustor development for hydrogen-rich gas turbine applications, *International Journal of Hydrogen Energy*, 44, 6978–6990.
- Kim W.W., Menon S., 1995, A new dynamic one-equation subgrid-scale model for large eddy simulations, 33rd Aerospace Sciences Meeting and Exhibit, 9-12 January 1995, Reno, United States.
- Li Z., Ferrarotti M., Cuoci A., Parente A., 2018, Finite-rate chemistry modelling of non-conventional combustion regimes using a Partially-Stirred Reactor closure: Combustion model formulation and implementation details, *Applied Energy*, 225, 637–655.
- Mashruk S., Kovaleva M., Chong C. T., Hayakawa A., Okafor E. C., Valera-Medina A., 2021, Nitrogen Oxides as a By-product of Ammonia/Hydrogen Combustion Regimes, *Chemical Engineering Transactions*, 89, 613–618.
- Mével R., Javoy S., Lafosse F., Chaumeix N., Dupré G., Paillard C. E., 2009, Hydrogen-nitrous oxide delay times: Shock tube experimental study and kinetic modelling, *Proceedings of the Combustion Institute*, 32, 359–366.
- Spalding D.B., 1977, Development of The Eddy Break-Up Model of Turbulent Combustion, 16th Symposium (International) on Combustion, 1657–1663, 15-20 August 1976, Cambridge, United States.
- Tacke M. M., Linow S., Geiss S., Hassel E. P., Janicka J., Chen J. Y., 1998, Experimental and Numerical Study of a Highly Diluted Turbulent Diffusion Flame Close to Blowout, 27th Symposium (International) on Combustion, 1139–1148, 2-7 August 1998, Boulder, United States.
- Tekgöl B., Peltonen P., Kahila H., Kaario O., Vuorinen V., 2021, DLBFoam: An open-source dynamic load balancing model for fast reacting flow simulations in OpenFOAM, *Computer Physics Communications*, 267.
- Zhou X., Jiang X., Martinez D. M., 2016, The effects of chemical kinetic mechanisms on large eddy simulation (LES) of a nonpremixed hydrogen jet flame, *International Journal of Hydrogen Energy*, 41, 11427–11440.